

Journal of Biomedical Optics

BiomedicalOptics.SPIEDigitalLibrary.org

Optical mammography: bilateral breast symmetry in hemoglobin saturation maps

Pamela G. Anderson
Angelo Sassaroli
Jana M. Kainerstorfer
Nishanth Krishnamurthy
Sirishma Kalli
Shital S. Makim
Roger A. Graham
Sergio Fantini

Optical mammography: bilateral breast symmetry in hemoglobin saturation maps

Pamela G. Anderson,^a Angelo Sassaroli,^a Jana M. Kainerstorfer,^{a,†} Nishanth Krishnamurthy,^a Sirishma Kalli,^b Shital S. Makim,^b Roger A. Graham,^c and Sergio Fantini^{a,*}

^aTufts University, Department of Biomedical Engineering, 4 Colby Street, Medford, Massachusetts 02155, United States

^bTufts Medical Center, Department of Radiology, 800 Washington Street, Boston, Massachusetts 02111, United States

^cTufts Medical Center, Department of Surgery, 800 Washington Street, Boston, Massachusetts 02111, United States

Abstract. We present a study of the bilateral symmetry of human breast hemoglobin saturation maps measured with a broadband optical mammography instrument. We have imaged 21 patients with unilateral breast cancer, 32 patients with unilateral benign lesions, and 27 healthy patients. An image registration process was applied to the bilateral hemoglobin saturation (SO_2) images by assigning each pixel to the low, middle, or high range of SO_2 values, where the thresholds for the categories were the 15th and 85th percentiles of the individual saturation range. The Dice coefficient, which is a measure of similarity, was calculated for each patient's pair of right and left breast SO_2 images. The invasive cancer patients were found to have an average Dice coefficient value of 0.55 ± 0.07 , which was significantly lower than the benign and healthy groups (0.61 ± 0.11 and 0.62 ± 0.12 , respectively). Although differences were seen in a group analysis, the healthy patient Dice coefficients spanned a wide range, limiting the diagnostic capabilities of this SO_2 symmetry analysis on an individual basis. Our results suggest that for assessing the SO_2 contrast of breast lesions, it may be better to select a reference tissue in the ipsilateral rather than the contralateral breast. © The Authors. Published by SPIE under a Creative Commons Attribution 3.0 Unported License. Distribution or reproduction of this work in whole or in part requires full attribution of the original publication, including its DOI. [DOI: [10.1117/1.JBO.21.10.101403](https://doi.org/10.1117/1.JBO.21.10.101403)]

Keywords: optical mammography; breast cancer; symmetry; Dice coefficient.

Paper 150690SSR received Oct. 15, 2015; accepted for publication Jan. 13, 2016; published online Feb. 5, 2016.

1 Introduction

Near-infrared spectroscopy (NIRS) and diffuse optical imaging (DOI) utilize light in the wavelength range of 600 to 1000 nm to characterize the breast optical properties and to generate images based on the absorption and scattering properties of breast tissue. Using NIRS techniques, the tissue concentrations of oxy-hemoglobin, deoxyhemoglobin, water, and lipids (denoted as [HbO], [Hb], [water], and [lipid], respectively) can be found in the breast. Hemoglobin saturation (SO_2) is another parameter that can also be optically measured. SO_2 is a ratio of [HbO] to total hemoglobin concentration ([HbT]), indicating the balance between the perfusion per unit time per unit volume of tissue and the rate of oxygen consumption due to metabolic activity. Here, we investigate the bilateral symmetry in optical breast imaging, specifically in SO_2 images, for healthy patients and for patients with benign and malignant breast lesions.

1.1 Bilateral Breast Symmetry in X-Ray Imaging and Thermography

Symmetry between right and left breasts is an important consideration when interpreting breast images in x-ray mammography.^{1,2} A study investigating breast density patterns

on x-ray mammograms reported symmetry between 30 women's left and right breasts using both subjective and objective measurements schemes.³ Subjective measures of symmetry were performed by radiologists grading the percentage of dense breast tissue in six categories (none, 0% to 10%, 10% to 25%, 25% to 50%, 50% to 75%, 75% to 100%) and comparing the grade given for right and left breast mammograms.³ As for an objective bilateral symmetry assessment, one method was to find the skewness parameter from the histogram of the gray-scale pixel values in the digitized mammograms for each breast.³ Bilateral symmetry was reported for both subjective and objective measurement types, with a general result that the x-ray images of a woman's two breasts show a significant level of symmetry.³ Making use of such symmetry in healthy breasts, multiple x-ray mammography studies have implemented image registration techniques using bilateral subtraction to attempt to improve the detection of suspicious masses.⁴⁻⁶ Different registration and subtraction methods have been proposed, which vary in the alignment technique, the complexity of image deformation approach, and the segmentation process.⁴⁻⁶ However, when asymmetric appearance is found between right and left x-ray mammograms, it is considered to be a potential marker for cancer and it is carefully assessed by radiologists. In a study of over 8000 mammograms, it has been reported that only 3% of the cases were assessed by radiologists to have asymmetric breast tissue,² which indicates the high amount of similarity often seen between two breasts' mammographic appearances. This study did include asymptomatic and symptomatic women, however, any mammograms found with masses, microcalcifications, or architectural distortions were omitted

*Address all correspondence to: Sergio Fantini, E-mail: sergio.fantini@tufts.edu

[†]Present address: Carnegie Mellon University, Department of Biomedical Engineering, 700 Technology Drive, Pittsburgh, Pennsylvania 15219, United States.

from the analysis.² Examining the symmetry in one breast over time is also performed in mammography and is used for identifying developing asymmetries.⁷ Longitudinal comparisons with prior mammograms offer the advantage of looking at changes occurring within the same breast for screening and diagnostic purposes.

Another imaging modality that relies on bilateral symmetry qualities in healthy patients is breast thermography. Thermography is an imaging modality that measures the temperature distribution over the breast, which is influenced by perfusion within the tissue. Studies in breast thermography have introduced methods for segmentation and symmetry analysis in efforts to distinguish healthy and diseased patients.^{8,9} Characteristics measured from the bilateral thermograms, such as mean temperature or the histogram qualities of the temperature distribution within the thermogram, serve as inputs to classification techniques to assess asymmetry for cancer detection purposes.⁹ Understanding and characterizing symmetric qualities between right and left breasts in healthy individuals can provide useful indicators when developing symmetry-based methods for disease detection.

1.2 Optical Breast Imaging

Optical imaging studies have examined the spatial variation in chromophore concentrations and SO_2 in the healthy breast. Using NIRS tomography and magnetic resonance imaging, Brooksby et al.¹⁰ investigated the variations in the different types of healthy breast tissue by measuring the properties of fibroglandular and adipose tissue. A significantly higher concentration of [HbT], [water], and scattering amplitude and power were found in fibroglandular tissue when compared with adipose tissue. (Scattering amplitude relates to the absolute value of the tissue reduced scattering coefficient, while scattering power refers to its wavelength dependence.) The average values of [HbT] and [water] in fibroglandular tissue were reported to be $22.4 \pm 7.3 \mu\text{M}$ and $60.3\% \pm 23.6\%$, respectively, whereas in adipose tissue [HbT] and [water] were found to be $17.1 \pm 3.1 \mu\text{M}$ and $46.8\% \pm 18.5\%$, respectively.¹⁰ The higher amount of [HbT] and [water] in fibroglandular tissue is expected due to the increase in tissue density and vascularity. The only parameter that did not show a statistically significant difference between the two types of tissue was SO_2 .¹⁰ Similarity in each of the four quadrants of one breast and bilateral symmetry have been investigated by Shah et al.¹¹ when measuring 28 healthy patients with a handheld optical probe. The chromophore concentrations, SO_2 , and scattering parameters within each breast quadrant and the nipple areolar complex (NAC) were determined.¹¹ The difference in the magnitude of the chromophore concentrations and scattering parameters was reported between symmetric regions of the right and left breasts. The largest average difference between any two of the four symmetric quadrants was 31% in [HbT], indicating the inherent variations in hemoglobin concentration that may exist between a patient's two breasts.¹¹ Because of such intrinsic spatial variability in the breast optical properties, Shah et al. expressed concern in using the symmetric region of the contralateral breast as a reference for contrast measurements.¹¹ Optical imaging methods have also found that within healthy breast tissue there are expected variations in chromophore concentrations and scattering properties.

1.3 Importance of Symmetry in Optical Imaging

Bilateral symmetry in optical mammograms can be examined for healthy, benign, and cancer patients. Since SO_2 has been found to not show a significant difference between different types of healthy breast tissue,¹⁰ bilateral variations in this parameter could be explored for disease detection purposes. Symmetry will not just take into account the average SO_2 value within the breast but also its spatial distribution. Therefore, even if healthy tissue has a wide range of SO_2 values, the similarity between the spatial distributions in the patient's two maps may prove to be an important indicator of health. The presence of a lesion may cause one breast to feature a localized perturbation and therefore deviate from the spatial distribution of SO_2 in the contralateral breast. Additionally, examining the bilateral symmetry in optical images of healthy patients can provide useful information to help determine if the contralateral breast is the appropriate selection for the reference tissue when measuring lesion contrast. Many NIRS studies have focused on the optical characterization of breast cancer^{12–24} and monitoring tumor response to neoadjuvant chemotherapy.^{25–30} A crucial aspect of these studies is how the tumor contrast is measured. It has been well established that, due to angiogenesis, the concentration of hemoglobin in cancerous tissue is consistently greater compared with healthy breast tissue. However, when measuring the SO_2 contrast, the results have been inconsistent. Some studies have found that the SO_2 within a tumor is lower compared with healthy tissue,^{19–22,24} whereas others found no significant difference between the SO_2 in tumors and healthy tissue.^{12,15–17,23,31} The choice of reference tissue for the contrast calculations also differs across the studies; some consider the background area surrounding the lesion^{15,17,19,21,31} and others the tissue in the mirrored region of the contralateral breast.^{12,20} Characterizing the spatial distribution of SO_2 in the right and left breasts of healthy patients will help quantify the level of bilateral symmetry. If healthy breasts' SO_2 maps are found to be highly symmetric, this would validate the choice of the contralateral breast for reference tissue selection when characterizing the SO_2 contrast of a lesion. Otherwise, a lack of symmetry between right and left healthy breasts would question such a choice, indicating a potentially better choice of reference tissue within the same breast.

In this work, we examine the bilateral symmetry of the hemoglobin saturation maps of healthy patients and patients with benign or malignant lesions. The image pixels in the left and right maps are first labeled as high, middle, or low SO_2 values, and the left and right images are then quantitatively compared with one another to evaluate their degree of symmetry. The aim of this study is to characterize the degree of bilateral symmetry for the SO_2 breast maps of healthy subjects and determine whether the presence of benign or cancerous breast lesions impacts such degree of symmetry.

2 Methods

2.1 Patient Measurements

A broadband, continuous-wave optical mammography instrument was used to image the patients in this study. A detailed description of the instrument can be found in Anderson et al.²⁴ Briefly, the system scans a source optical fiber and a detector optical fiber in tandem over two parallel polycarbonate plates between which the breast is mildly compressed. A xenon arc lamp source (Model No. 6258, Newport Corporation, Irvine,

California) is filtered to emit wavelengths from 650 to 950 nm, and a spectrograph (Model No. SP-150, Princeton Instruments, Acton, Massachusetts) and charge-coupled device (CCD) camera (Model No. DU420A-BR_DD, Andor Technology, South Windsor, Connecticut) are used to spectrally disperse and measure the transmitted light. Each scan is performed in craniocaudal view and the transmission spectra are acquired every 2 mm along the x and y coordinates over the area of the breast. The transmission spectra are processed with a continuous-wave, diffusion-based model for a slab geometry,³² which is used as the forward solver in an inversion procedure based on the Levenberg-Marquardt method.³³ The model's implementation is further described in Anderson et al.²⁴ With this model, the tissue concentrations of deoxyhemoglobin, oxyhemoglobin, water, and lipids are recovered at each breast pixel. The scattering amplitude, i.e., the reduced scattering coefficient at a reference wavelength [$\mu'_s(\lambda_0)$], and the scattering power, i.e., the exponent of the power law dependence of the reduced scattering coefficient on the wavelength (b), were fixed in the model to average values reported in the literature [$\mu'_s(670 \text{ nm}) = 10.5 \text{ cm}^{-1}$, $b = 1.00$].³¹ Fixing the scattering parameters is necessary in order to achieve a unique solution for the chromophore concentrations.³⁴

In this study, we imaged the right and left breasts of 80 patients. Twenty-seven patients were classified as healthy, with no breast abnormalities found on x-ray mammography. A total of 32 patients had benign lesions identified by x-ray mammography, and the remaining 21 patients had biopsy-proven breast cancer. We required at least one week to go by before imaging patients who had already received a biopsy ($n = 9$) to minimize effects the procedure may have on the optical mammograms.¹⁷ This study was approved by the Institutional Review Board at Tufts Medical Center. Written informed consent was obtained from each patient before participating in the study.

2.2 Correlation among Retrieved Parameters

The continuous-wave, diffusion-based model solved for the tissue concentrations of the four chromophores, and, additionally, for a so-called amplitude parameter.²⁴ The amplitude parameter, also referred to in the literature as amplitude factor,³⁵ served as a scaling factor to best match the magnitude of the measured breast transmission spectra to the calculated data with the model. The mathematical model expressed the attenuation of power per unit area of the detector, i.e., the intensity at the detector divided by the input source power. In the case of *in vivo* measurements, which deviate from the ideal model conditions of a homogeneous medium and infinite slab geometry, a positive correlation was observed between the amplitude parameter and the chromophore concentrations. When we fit for the amplitude parameter, [Hb], [HbO], [water], and [lipid] for a breast cancer patient's data, we consistently found that the recovered amplitude parameter in the tumor region was smaller than the recovered amplitude parameter in the healthy tissue. This is because the amplitude parameter plays a role in compensating for the violation of some of the model's assumptions (i.e., slab geometry and homogeneous tissue) in order to find a minimum of the cost function in the inversion procedure. In addition to the inevitable partial volume effects from the analysis of a localized absorber with a homogeneous medium model, the positive correlation between the amplitude parameter and chromophore concentrations resulted in the recovered absorption contrast of the tumor to be much lower than expected. This result prompted

us to fix the amplitude parameter in order to retrieve better estimates of the optical parameters of breast lesions.

There are several measurable quantities that factor into the amplitude parameter: the source power, the size and numerical aperture of the source and detector optical fibers, the optical coupling efficiency between tissue and optical fibers, the level of f -number matching between the detector optical fiber and the spectrograph, and the sensitivity of the CCD camera. There are also variables that affect the amplitude parameter that cannot be estimated at each scanned pixel. For example, the optical power penetrating into the tissue at every pixel depends on the nature of the mechanical contact and pressure between breast tissue and the imager plates. Due to the curved geometry of the breast, this mechanical coupling is variable over the imaged breast area. The plate coupling and breast geometry also impact the measured intensity at the detector, resulting in another variable that affects the amplitude parameter. While all of these factors do affect the amplitude parameter, a major effect is also due to the presence of optical inhomogeneities within the breast.

To understand what effect inclusions of various sizes and optical properties have on the recovered parameters from a fit with a homogeneous slab model, we used transmittance data computed from a homogeneous medium model³² and from a perturbation model³⁶ (both in an infinite slab geometry, with slab thickness 6 cm) to solve for the amplitude parameter and the chromophore concentrations. In the perturbation case, we considered cubic perturbations (sides: 1.0, 2.4 cm) aligned with the source and detector, and embedded in the otherwise homogeneous medium 2 cm below the surface. The optical properties of the homogeneous medium (which are also the optical properties of the background medium for the perturbation case) at the reference wavelength of 650 nm are absorption coefficient $\mu_a = 0.05 \text{ cm}^{-1}$, reduced scattering coefficient $\mu'_s = 9.9 \text{ cm}^{-1}$, and scattering power $b = 1$. The optical perturbations considered, feature optical properties that are the same (\rightarrow), smaller (\downarrow), greater (\uparrow), or much greater ($\uparrow\uparrow$) than those of the background medium. More specifically: $\uparrow\mu_a = 0.06 \text{ cm}^{-1}$, $\uparrow\uparrow\mu_a = 0.14 \text{ cm}^{-1}$, $\downarrow\mu'_s = 7.6 \text{ cm}^{-1}$, $\uparrow\mu'_s = 10.7 \text{ cm}^{-1}$, and $\uparrow b = 1.35$. The $\uparrow\mu_a$ perturbations are intended to mimic breast cancer, whereas the $\uparrow\mu_a$, $\downarrow\mu'_s$, and $\uparrow b$ perturbations are intended to mimic intrinsic tissue heterogeneities, such as represented by the optical contrast between fibroglandular and adipose tissue.¹⁰

2.3 Image Registration and Dice Coefficient

Using the two-dimensional (2-D) optical breast images from healthy patients and from patients with benign and malignant lesions, we investigated the bilateral symmetry of the hemoglobin saturation maps. A linear registration was performed using a patient's left and right breast SO_2 maps by first mirroring the left breast image so that the medial and lateral sides corresponded in both breast maps. Then the same number of rows in each image, beginning with the top edge of the nipple region and extending towards the chest wall, were kept. Next, the center pixel of the row closest to the chest wall for each map was aligned and any remaining pixels along the outside borders that did not overlap were cut from the maps. The two SO_2 maps for the right and left breast then had the same number of pixels and the same shape. The average percentage of pixels that were kept from the two maps was 84.1%. An example of a healthy patient's map registration is shown in Fig. 1, where the gray pixels are cut from

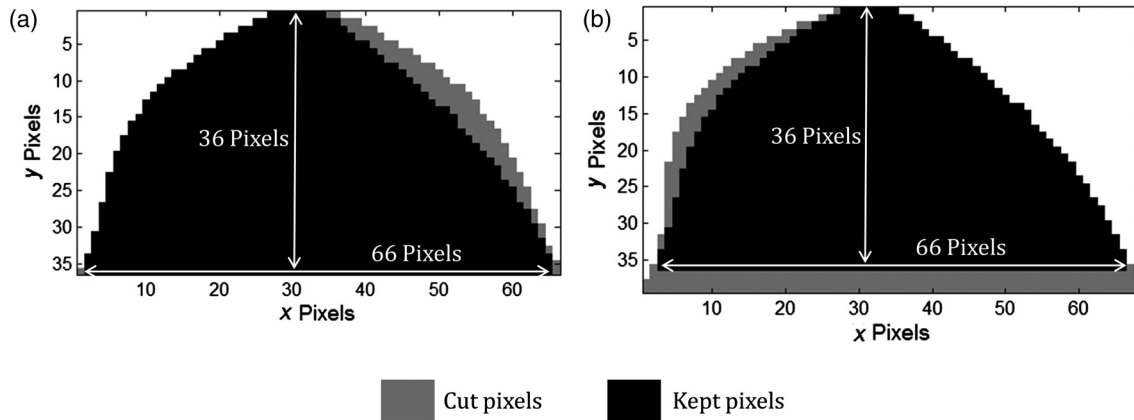


Fig. 1 A representative case illustrating how two images are registered. Starting from the nipple areas of the left and right breast, the same number of rows (parallel to the x axis) are kept and any remaining rows toward the chest wall are removed (low area of the RCC image in this case). The maps are then overlaid with the center points of the last rows (toward the chest wall) aligned, and any pixels along the borders that do not overlap are removed. LCC: left craniocaudal; RCC: right craniocaudal. (a) Mirrored LCC size map and (b) RCC size map.

each image and the black pixels are kept. The benign and cancer patients only had unilateral lesions. The 32 patients with benign lesions were then grouped into three different risk categories as described in Guray and Sahin.³⁷ Risk category 1 corresponds to nonproliferative lesions³⁷ or lesions that had been assessed as benign because of their stability on the x-ray mammogram (over 2 years). Risk categories 2 and 3 correspond to benign proliferative lesions without and with atypia, respectively.³⁷ The demographic for patients within each category are shown in Table 1. Two patients in the benign group did not have biopsy information available and therefore were not grouped into a subcategory. The symmetry of right and left breast SO_2 maps was then examined for cancer, benign (subcategorized by risk category), and healthy patient data.

The degree of symmetry between the SO_2 maps of a patient's right and left breast was quantified using the Dice coefficient. The Dice coefficient is a measure of similarity of two samples or, in our case, two images. By identifying A and B with the two SO_2 images (right and left breast), the Dice coefficient can be defined as follows:³⁸

$$\text{Dice coefficient} = \frac{2N(A \cap B)}{N(A) + N(B)}, \quad (1)$$

Table 1 Patient information organized by subcategory.

Group	Subcategory	Number of patients	Average age (yr)	Average BMI (kg/m^2)
Cancer	Invasive carcinoma	18	58 ± 11	28 ± 7
	<i>In situ</i> carcinoma	3	51 ± 7	29 ± 8
Benign	Proliferative with atypia	2	59 ± 10	28 ± 6
	Proliferative without atypia	8	44 ± 18	24 ± 5
	Nonproliferative	20	48 ± 5	28 ± 1
Healthy	Healthy	27	54 ± 11	26 ± 5

where $N(A)$ and $N(B)$ are the numbers of pixels in the SO_2 images of the right and left breasts ($N(A) = N(B)$ in our case), and $N(A \cap B)$ is the number of pixels with matching SO_2 labels in the two images. Instead of using the actual values of SO_2 within the resized maps, each pixel was labeled as low saturation, middle saturation, or high saturation. These labels were defined by finding the SO_2 values that represent the 15th and the 85th percentiles of the saturation value distribution for the SO_2 pixels, and using these percentiles as cutoffs between the three groups. These percentiles were chosen so that low saturation pixels (identifying relatively hypoxic areas indicative of a potential imbalance of perfusion and metabolic rate) and high saturation pixels (identifying relatively hyperoxic areas) get grouped together. The largest number of pixels (70% of the total) was assigned to the middle range of SO_2 values. After the pixels in the left and right SO_2 maps were labeled, $N(A \cap B)$ was calculated as the number of pixels that fell in the same SO_2 range (low, middle, or high) in congruent locations for right and left breast images. The Dice coefficient can take values between 0 and 1, with higher values corresponding to a greater degree of symmetry between the right and left SO_2 images.

3 Results

3.1 Correlation among Retrieved Parameters

The transmittance data computed with the homogeneous medium and perturbation forward models, as described in the Methods section, were used to determine the effect of optical perturbations on the recovered amplitude parameter from the fit with the homogeneous medium model. When using spectra calculated from the homogeneous forward model in a 6-cm-thick slab geometry (with the amplitude parameter set to 1), the inversion procedure recovered the correct amplitude parameter as shown in Fig. 2 (first point). For transmittance data generated with a small perturbation (1 cm), there was not a major effect on the recovered amplitude parameter (overestimated by 2%; sixth point in Fig. 2). For the data computed with a large perturbation having properties representing the contrast between fibroglandular and adipose tissue, the model overestimated the amplitude parameter by 12.5% (seventh point in Fig. 2). This

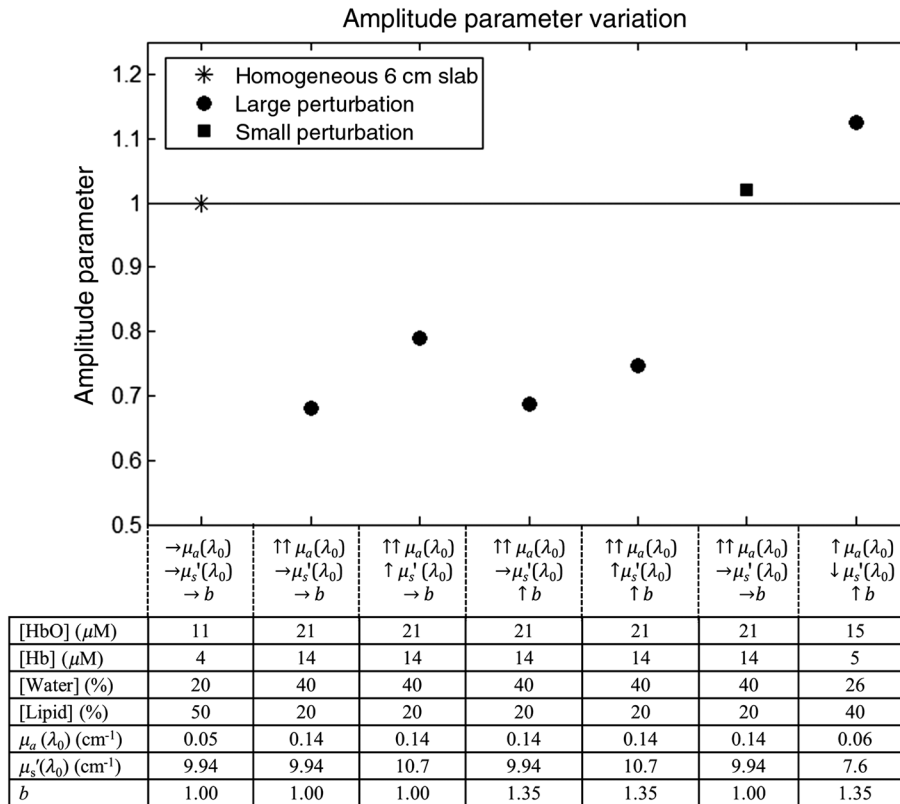


Fig. 2 Recovered amplitude parameter found by fitting the computed transmittance data with the homogeneous slab model. The reported values are the chromophore concentrations and scattering parameters used for the background (1st point on x-axis) and localized perturbations (2nd to 7th point on x-axis). The reference wavelength, λ_0 , is 650 nm. Small perturbation: cube with 1.0 cm side. Large perturbation: cube with 2.4 cm side.

increase in the recovered amplitude parameter is due to the decrease in $\mu_s'(\lambda_0)$ within the perturbation. The lower amplitude parameter that has been observed in patient data was reproduced in the curves with the 2.4-cm perturbations (large perturbations) with a large ($\uparrow\uparrow$) increase in μ_a (second to fifth points in Fig. 2). The recovered amplitude parameter was consistently underestimated by over 20% as seen in Fig. 2. This underestimation occurred regardless of whether the reduced scattering coefficient (μ_s') and the scattering power (b) of the perturbation were the same or higher than those of the background medium. Due to the positive correlation between the amplitude parameter and the chromophore concentrations (which are directly linked to μ_a), the chromophore concentrations were also underestimated. Since we are using a homogeneous model to fit the transmission optical data through an inhomogeneous medium, it is not expected that the exact concentrations of the perturbation are retrieved, even though a correct relative direction (higher or lower concentration than the background) is expected. When we did not fix the amplitude parameter, the data for the large perturbation with $\uparrow\uparrow \mu_a$, $\rightarrow \mu_s'(\lambda_0)$, and $\rightarrow b$ result in recovering only a 10% increase in [HbT] compared with the background tissue. By fixing the amplitude parameter to 1, the [HbT] contrast increases to 30% (the actual contrast in [HbT] was 133%).

Based on the aforementioned computed results reported, there is a greater underestimation of the amplitude parameter for larger perturbations, which will impact the *in vivo* data. Lower absorption contrast will be found when fitting chromophore concentrations and amplitude parameter in regions with

large malignant or benign lesions that feature a strong optical contrast. Therefore, we have decided to fix the amplitude parameter at the same value for all pixels in the right and left breast images. This value was given by the average amplitude parameter over the healthy breast (or both healthy breasts in the case of healthy patients) to recover a more accurate chromophore contrast for optical inhomogeneities in the breast. Of course, fixing the amplitude parameter to the healthy breast's average value causes the model fits to be slightly worse (i.e., resulting in a greater minimized value of the cost function) than when the amplitude parameter is being retrieved.

3.2 SO_2 Bilateral Symmetry

To investigate the symmetry between the SO_2 maps of the left and right breasts, the registration method was applied to all 80 patients (27 healthy, 32 with benign lesions, and 21 with cancer). Figure 3 shows an example of a healthy patient's right and left breast SO_2 maps. The black outlines within each map depict the borders that separate the regions of high, middle, and low saturation, which were labeled using the 15th and 85th percentile values. The congruence map is shown on the bottom panel of Fig. 3, displaying the pixels where the SO_2 labels were either matching in both breasts (white for the high range, light gray for the middle range, dark gray for the low range) or nonmatching (black). This healthy patient had a Dice coefficient of 0.84, which indicates a high degree of bilateral symmetry in the hemoglobin saturation maps.

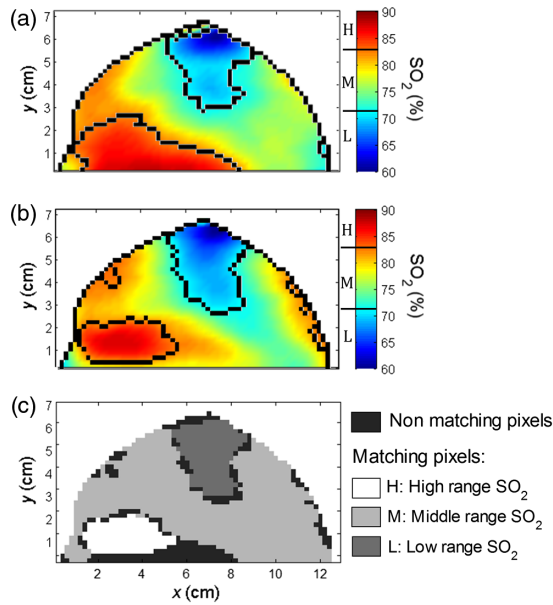


Fig. 3 Example of a resized (a) right breast map, (b) mirrored left breast map, and (c) congruence map calculated for a healthy 34-year-old patient (patient index: 70) whose SO_2 maps demonstrate a high level of bilateral symmetry. The black contour lines divide the three labeled regions of low (“L”), middle (“M”) and high (“H”) SO_2 values found from the 15th and 85th percentile thresholds. The congruence map shows the matching and nonmatching pixels and is characterized by a Dice coefficient of 0.84.

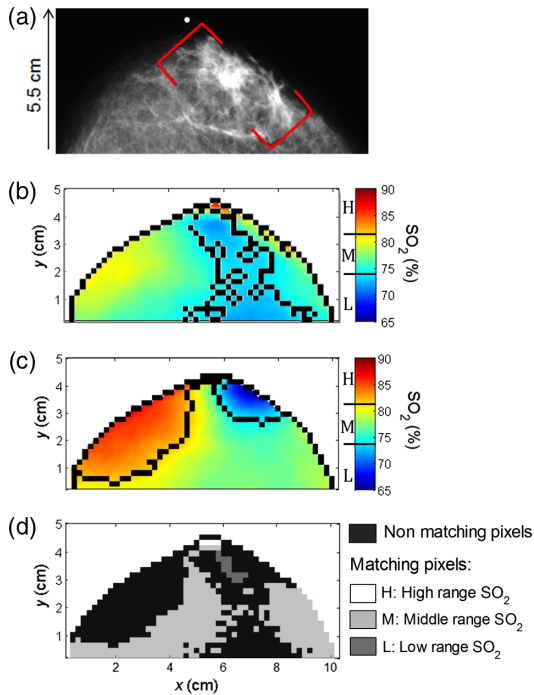


Fig. 4 Images for a cancer patient (patient index: 13) who has a 5 cm invasive lobular carcinoma in her right breast laterally. (a) The x-ray mammogram shows two red brackets drawn by the radiologist indicating where the invasive lobular carcinoma is located. SO_2 maps for this patient’s (b) cancerous right breast and (c) mirrored left breast are found below. The black contour lines divide the three labeled regions of low (“L”), middle (“M”), and high (“H”) SO_2 values found from the 15th and 85th percentile thresholds. (d) The congruence map shows the matching and nonmatching pixels. This patient was found to have a Dice coefficient of 0.46.

Figure 4 displays the x-ray mammogram and SO_2 maps for a patient with a 5-cm invasive lobular carcinoma laterally in her right breast. The congruence map for this cancerous patient shows many nonmatching pixels and this patient was found to have a Dice coefficient of 0.43, consistent with a low degree of bilateral symmetry.

The Dice coefficients for the breast cancer patients (patient index: 1 to 21) are plotted in Fig. 5, and their average value was found to be 0.57 ± 0.07 (standard deviation). When the Dice coefficients for the three patients who were diagnosed with ductal carcinoma *in situ* (DCIS) were excluded, the group average slightly decreased to 0.55 ± 0.07 . The average Dice coefficients for the patients with benign lesions (patient index: 22–51) was 0.61 ± 0.11 . This group was subdivided into three risk categories, low risk (category 1), middle risk (category 2), and high risk (category 3). There were two patients in the benign group (patient index: 79, 80, data not shown in Fig. 5) for whom we did not have biopsy information available; therefore, they are not included in this stratified analysis. The 20 low-risk benign lesion patients had an average Dice coefficient of 0.65 ± 0.09 . Patients in risk categories 2 and 3 had average Dice coefficients of 0.56 ± 0.08 and 0.45 ± 0.01 , respectively. It is important to note, however, that risk category 2 included eight patients and risk category 3 only two patients. The healthy patients (patient index: 52 to 78) had an average Dice coefficient of 0.62 ± 0.12 . Table 2 reports the average Dice coefficients and standard deviations for each group. To determine if the group averages were different from one another, we performed a Wilcoxon rank sum test. The Dice coefficients for the group of cancer patients, not including DCIS patients, were found to be significantly different from the Dice coefficients for the benign and healthy patients ($p < 0.05$). When including the DCIS patients in the cancer group, the p values found from the statistical test were just above 0.05. The box plot in

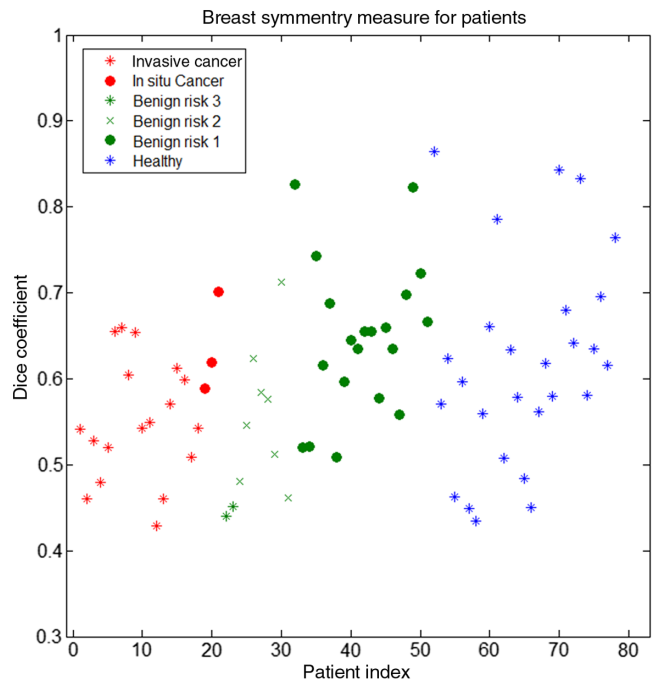


Fig. 5 Dice coefficients for each patient group. Cancer, benign, and healthy patients have patient indices 1 to 21, 22 to 51, and 52 to 78, respectively.

Table 2 Average values of the Dice coefficients for different patient groups. The p values found from the Wilcoxon rank sum test are also shown, where “ref” represents the reference patient group to which the others are compared.

	Dice coefficient	p value (ref: benign)	p value (ref: healthy)
Cancer (no DCIS)	0.55 ± 0.07	0.024	0.023
Cancer (with DCIS)	0.57 ± 0.08	0.051	0.0525
Benign	0.61 ± 0.11	—	0.51
Healthy	0.62 ± 0.12	0.50	—

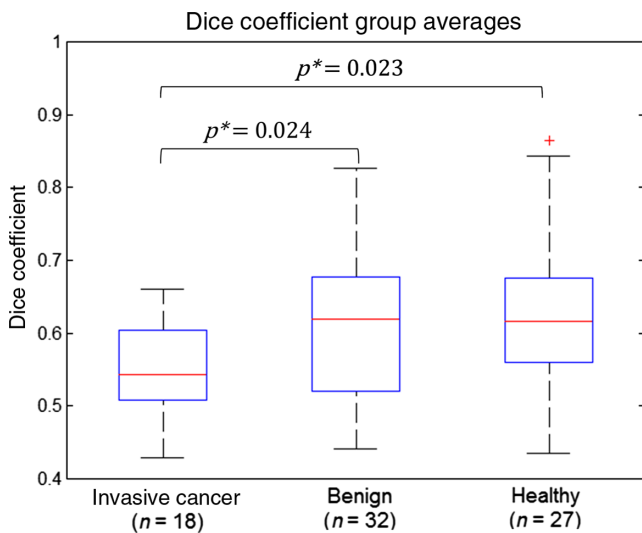


Fig. 6 The box plot above illustrates the Dice coefficient average for the invasive cancer patients, patients with benign lesions, and healthy patients. The p values were found by using the Wilcoxon rank sum test.

Fig. 6 represents the median value in each group and the box edges extend to the 25th and 75th percentile. The line coming out of the box shows the extreme points for each patient group. Figure 6 portrays the lower average Dice coefficient for the invasive cancer group when compared with the benign and healthy patient groups.

4 Discussion

4.1 Group Analysis of the Dice Coefficient

The Dice coefficient provides a quantitative metric to compare the similarity between the right and left breast hemoglobin saturation maps. Further details of each patient imaged in this study are included in Table 3. Although the average Dice coefficient for patients with invasive carcinoma was significantly lower when compared with that of the benign and healthy groups, Fig. 5 demonstrates that this could not be used diagnostically on an individual basis due to the large overlap between the ranges of Dice coefficients for the three groups. However, some level of stratification can be found amongst the cancer and benign patients groups. While there are only a small number of DCIS cases, it can be seen in Fig. 5 that those three patients

(patient index: 19 to 21) have higher Dice coefficient values (average: 0.64) compared with the other invasive carcinoma patients (average Dice coefficient: 0.55). Within the benign patient group, patients with higher risk lesions (risk category 2 and 3) had lower Dice coefficients than patients in risk category 1. This difference would support the hypothesis that the asymmetry between the SO_2 maps increases with the complexity of the breast lesion, perhaps due to the increased metabolic requirements associated with increased proliferation and the development of atypia. Unfortunately, the small sample size of patients with benign lesions in risk category 2 and 3 limits the significance of this result. When performing a power analysis with $\alpha = 0.05$ and $\beta = 0.9$, we found that our study would have required a total of 23 high risk (category 2 and 3) patients to potentially obtain a significant result between the low risk and high risk patients. Further recruitment would therefore be needed in order to confirm this initial observation. Within the benign risk category 1 group (nonproliferative lesions) there were three patients who were found to have cysts. Cysts have been reported to have lower SO_2 values,¹⁴ however, the three patients exhibited average values of Dice coefficients (0.69, 0.60, 0.66) when compared with other nonproliferative lesions. Therefore, the presence of cysts did not indicate any increased asymmetry.

The Dice coefficients for the healthy patient group span a wide range of values, thus demonstrating that simple asymmetry of a patient's SO_2 maps does not necessarily correlate with a specific disease process. There was a cluster of six healthy patients with Dice coefficients of 0.51 or below, and a longitudinal study would be required to see if this degree of dissimilarity has always been present or has developed overtime. We examined several factors to determine if the Dice coefficients of healthy patients have any relation to other known parameters. We found no significant correlation between the Dice coefficients and the patients' age, menopausal status, or average plate separation (maximum thickness of the imaged breast). We also tested to determine whether there was a trend between the Dice coefficient and the difference between the maximum thicknesses in the right and left breast and found none. Even though this method could be applied to other parameters, we have focused on the bilateral symmetry in SO_2 maps because hemoglobin saturation is a ratio and less sensitive to the geometrical artifacts from the breast shape that can be present in parallel plate geometry.

4.2 Reference Tissue

The range in similarity and dissimilarity between the SO_2 maps of healthy patients raises questions on the appropriateness of using the mirror region of the contralateral breast as the reference tissue for the characterization of the optical contrast of benign or malignant breast lesions. The contralateral breast seems advantageous to use as the reference tissue because there is no concern about a tumor impacting the measurement, the tissue is easily accessible, and it should reflect the healthy properties of that patient's breasts. Similarity between the spatial distributions of SO_2 in healthy right and left breasts would justify the use of the mirrored region in the contralateral breast for lesion characterization purposes. However, whether due to physiological asymmetries between the two breasts or to any measurement variation between the two scans, we did not find healthy SO_2 maps to feature any consistent level of bilateral symmetry. For certain patients (like the one depicted in Fig. 3),

Table 3 Information for the patients included in this study. The groups are categorized as cancer, benign, and healthy patients. Patient index refers to the numbering adopted in this work. Patient ref number is the number assigned at the time of enrollment in the study. The age, menopausal status, plate separation, height, and weight are also given for all patients (when data were available). The asterisk within the plate separation column indicates the side that has the breast lesion. The type of lesion is categorized as follows: risk 1 for benign nonproliferative disease; risk 2 for benign proliferative disease, and risk 3 for benign proliferative disease with atypia. Cancer types were also defined: IDC: invasive ductal carcinoma; DCIS: ductal carcinoma *in situ*; ILC: invasive lobular carcinoma; LCIS: lobular carcinoma *in situ*. Dice coefficients for each patient are shown in the last column.

Group	Patient index	Patient ref number	Age (yr)	Menopausal status	Plate sep (cm)*		Height (cm)	Weight (kg)	Type of lesion	Dice coef
					Left	Right				
Cancer	1	72	68	Post	5.5	5.5*	—	—	IDC/DCIS	0.54
	2	82	36	Pre	5.0*	5.0	150	45	IDC/DCIS	0.46
	3	116	51	Post	6.2	6.8*	175	120	IDC/DCIS	0.53
	4	125	66	Post	6.5	6.3*	178	82	IDC/DCIS	0.48
	5	128	59	Post	8.2*	6.3	175	66	ILC/LCIS	0.52
	6	133	52	Post	7.5	7.2*	170	113	IDC	0.66
	7	134	44	Post	7.5*	7.8	160	90	IDC	0.66
	8	137	66	Post	9.2*	7.2	165	108	IDC/DCIS	0.60
	9	141	63	Post	6.9*	6.4	175	82	IDC/DCIS	0.65
	10	143	76	Post	6.8*	6.6	152	54	IDC/DCIS	0.54
	11	146	48	Pre	6.6*	7.0	160	69	IDC/DCIS/LCIS	0.55
	12	149	75	Post	5.6	5.0*	178	67	IDC/DCIS	0.43
	13	150	72	Post	7.5	8.2*	157	57	ILC	0.46
	14	153	59	Post	6.3*	5.6	173	73	IDC	0.57
	15	154	48	Pre	7.4	7.4*	168	73	IDC/DCIS	0.61
	16	155	53	Pre	6.6	7.5*	170	85	ILC/DCIS/LCIS	0.60
	17	156	62	Post	7.0*	5.3	170	68	IDC	0.50
	18	157	49	Pre	6.6*	6.8	165	68	ILC/LCIS	0.54
	19	68	57	Post	6.5	6.0*	160	64	DCIS	0.59
	20	99	53	Post	5.5	5.0*	170	68	DCIS	0.62
	21	158	43	Pre	7.9*	8.1	155	91	DCIS	0.70
Benign	22	95	44	Pre	6.5*	6.5	178	88	Risk 3	0.44
	23	120	51	Post	7.2*	6.0	173	87	Risk 3	0.45
	24	86	81	Post	5.0	5.0*	155	61	Risk 2	0.48
	25	87	21	Pre	5.0	5.0*	157	51	Risk 2	0.54
	26	97	47	Post	7.0*	7.0	163	74	Risk 2	0.62
	27	100	41	Pre	5.6	5.3*	168	45	Risk 2	0.58
	28	102	30	Pre	6.4*	5.3	165	73	Risk 2	0.58
	29	110	34	Pre	4.2	4.5*	165	52	Risk 2	0.51
	30	122	48	Pre	5.8*	5.7	160	62	Risk 2	0.71

Table 3 (Continued).

Group	Patient index	Patient ref number	Age (yr)	Menopausal status	Plate sep (cm)*		Height (cm)	Weight (kg)	Type of lesion	Dice coef
					Left	Right				
	31	139	49	Post	8.6*	8.2	163	77	Risk 2	0.46
	32	25	45	Pre	7.6*	7.8	165	70	Risk 1	0.83
	33	31	62	Post	6.3	5.3*	157	57	Risk 1	0.52
	34	45	63	Post	7.5*	8.1	170	87	Risk 1	0.52
	35	51	68	Post	6.6*	7.5	152	65	Risk 1	0.74
	36	59	48	Pre	6.5	6.5*	157	70	Risk 1	0.62
	37	62	64	Post	5.4*	5.5	160	62	Risk 1	0.69
	38	74	63	Post	5.5	5.3*	147	56	Risk 1	0.51
	39	84	52	Pre	4.0*	4.0	168	62	Risk 1	0.60
	40	90	44	Pre	7.0*	7.0	168	110	Risk 1	0.64
	41	96	62	Post	6.0*	6.0	168	72	Risk 1	0.63
	42	98	53	Post	7.0	6.5*	160	68	Risk 1	0.66
	43	103	52	Post	7.1	6.7*	160	89	Risk 1	0.66
	44	107	74	Post	6.6*	6.3	170	78	Risk 1	0.58
	45	108	60	Post	5.0*	5.2	163	58	Risk 1	0.66
	46	112	69	Post	6.0*	6.0	160	75	Risk 1	0.63
	47	114	66	Post	6.1*	6.3	168	122	Risk 1	0.56
	48	117	65	Post	7.9	7.5*	155	78	Risk 1	0.70
	49	123	41	Pre	4.9*	5.2*	165	62	Risk 1	0.82
	50	140	79	Post	4.4	5.1*	163	59	Risk 1	0.72
	51	142	51	Post	7.9*	7.0	173	86	Risk 1	0.67
Healthy	52	23	54	Post	6.0	5.9	—	77	—	0.86
	53	24	46	Pre	6.1	6.9	157	59	—	0.57
	54	29	69	Post	4.8	4.7	165	63	—	0.62
	55	35	67	Post	6.4	6.4	160	57	—	0.46
	56	36	48	Pre	4.5	4.6	168	57	—	0.60
	57	37	45	Post	7.5	7.8	163	73	—	0.45
	58	40	55	Post	7.1	8.1	163	90	—	0.43
	59	41	65	Post	6.5	7.0	160	70	—	0.56
	60	42	56	Pre	5.6	5.9	155	50	—	0.66
	61	44	60	Post	6.6	6.1	—	63	—	0.79
	62	46	66	Post	7.5	7.5	170	69	—	0.51
	63	47	56	Post	5.2	5.0	163	59	—	0.63

Table 3 (Continued).

Group	Patient index	Patient ref number	Age (yr)	Menopausal status	Plate sep (cm)*		Height (cm)	Weight (kg)	Type of lesion	Dice coef
					Left	Right				
	64	48	55	Post	6.6	6.9	157	70	—	0.58
	65	49	47	Pre	4.9	4.6	157	50	—	0.48
	66	50	58	Pre	6.9	6.8	175	78	—	0.45
	67	53	71	Post	6.2	6.2	165	64	—	0.56
	68	55	65	Post	4.6	5.3	168	81	—	0.62
	69	56	73	Post	6.0	6.2	170	64	—	0.58
	70	58	34	Pre	6.5	6.2	163	67	—	0.84
	71	61	48	Pre	8.0	8.0	168	96	—	0.68
	72	63	54	Post	5.2	5.0	163	64	—	0.64
	73	78	37	Pre	5.0	5.0	160	57	—	0.83
	74	85	56	Post	6.5	7.0	140	67	—	0.58
	75	88	39	Pre	4.0	4.0	168	64	—	0.63
	76	92	49	Pre	6.5	6.0	170	66	—	0.70
	77	93	31	Pre	6.0	6.0	163	102	—	0.62
	78	121	42	Pre	6.9	6.7	152	64	—	0.76
Benign	79	131	61	Post	6.8	6.4	165	64	—	0.77
	80	135	45	Pre	6.7	6.7	155	57	—	0.45

the right and left breast SO_2 maps had a high degree of symmetry, and this could be a situation in which the contralateral tissue may be appropriate to use as a healthy reference region. However, for other patients, the contralateral tissue may not serve as an accurate reference tissue for lesion characterization, since bilateral contrast may be inherently present and introduce a confounding factor. We propose the use of healthy tissue in the ipsilateral breast as the reference measurement. The choice of the ipsilateral reference tissue could be an area of similar size selected on the opposite side of the breast from where the tumor is located. This method, however, poses challenges when the cancer is located at the center of the breast. Another method reported in previous work by Anderson et al. used the global background, which was defined as the entire tissue surrounding the cancerous region and can be applied to breast cancer cases regardless of the location of the tumor.²⁴

4.3 Robustness of Method

The robustness of the calculated Dice coefficient was tested by acquiring repeat measurements on two healthy patients after the initial set of scans (all within an hour). The registration process, the labeling technique, and the Dice calculation on the second set of craniocaudal images were then performed again. The Dice coefficient varied by at most 5% between the two sets of scans, showing the robustness in the calculation and reproducibility in

the procedure. Different labeling percentiles were also investigated to determine if there was one that best differentiated healthy and cancerous patients. We aimed to keep the middle SO_2 range the largest percentile span due to the fact that, for most cases, the majority of the breast represented healthy tissue. The other percentile ranges tested were 10/90 and 20/80. For both of these ranges, the p values found by the rank sum test when comparing the healthy and invasive carcinoma patients were greater than 0.05. Therefore, we opted for the 15/85 percentile labels, which resulted in the greatest separation between the Dice coefficients of the cancer and healthy patients.

4.4 Future Direction

The diagnostic potential of this method could be further explored by measuring a patient's bilateral symmetry over time and determining what factors influence the similarity between the two breasts' hemoglobin saturation maps. If a patient's Dice coefficient was found to be high one year and low the next, this could indicate an evolving asymmetric metabolic change that would require further evaluation. It is also necessary to address the limitations of this study. The inability to measure scattering properties with our continuous-wave instrument results in potential errors in the recovered absolute chromophore concentration in the breast tissue.²⁴ Therefore, we chose to focus on only the SO_2 parameter since it is a relative

quantity and can be compared between two breasts even if the scattering properties are fixed to inaccurate values. Another limitation was that our instrument only uses one source and one detector and we were restricted to comparing the asymmetry between 2-D images. Depth information and three-dimensional (3-D) reconstructions are able to provide more information about the breast tissue and lesion location and could be helpful when evaluating bilateral symmetry. The use of 3-D images in symmetry analysis may prove to have more diagnostic potential.

While the diagnostic capabilities of optical mammography may be limited, especially in a screening population, the field has shown promise for monitoring breast cancer patients' response to neoadjuvant chemotherapy. The idea of applying image registration and examining the symmetry in images from both the diseased and healthy breasts over time has not yet been explored in treatment monitoring studies. By collecting images of the healthy and cancerous breast throughout chemotherapy, the Dice coefficient can be measured from the start through the end of treatment. The trend in the Dice coefficient could then be examined to see if better responses result in more symmetric breast maps by the end of therapy. Investigating the bilateral symmetry between optical breast images provides a novel form of analysis.

5 Conclusion

In this work, we have developed a method to objectively compare the bilateral symmetry between breast hemoglobin saturation maps. Cancer, benign, and healthy patient groups were imaged and Dice coefficients were calculated as a measure of the bilateral symmetry. The SO_2 maps of patients with invasive cancer were shown to have a lower degree of similarity when compared with the maps of healthy patients or patients with benign lesions. However, the large range of Dice coefficients in healthy breasts limits the diagnostic potential of this method for individual patients. Additionally, the lack of bilateral symmetry of the SO_2 images in a number of healthy patients raises concerns regarding the use of the contralateral tissue as a reference selection for the characterization of the optical contrast of breast lesions.

Acknowledgments

We would like to thank Cate Mullen, RN, for her help recruiting patients for this study. We would also like to thank Paul Lapre for his help with the analysis. This research is supported by the National Institutes of Health (Grant R01 CA154774). This material is also based upon work supported by the National Science Foundation Graduate Research Fellowship (NSF DGE-0806676). Any opinion, findings, and conclusions or recommendations expressed in this material are those of the author (s) and do not necessarily reflect the views of the National Science Foundation.

References

1. E. A. Sickles, "Mammographic features of 'early' breast cancer," *Am. J. Roentgenol.* **143**(3), 461–464 (1984).
2. D. B. Kopans et al., "Asymmetric breast tissue," *Radiology* **171**(3), 639–643 (1989).
3. J. W. Byng et al., "Symmetry of projection in the quantitative analysis of mammographic images," *Eur. J. Cancer Prev.* **5**(5), 319–327 (1996).
4. F. F. Yin et al., "Computerized detection of masses in digital mammograms: analysis of bilateral subtraction images," *Med. Phys.* **18**(5), 955–963 (1991).
5. M. Y. Sallam and K. W. Bowyer, "Registration and difference analysis of corresponding mammogram images," *Med. Image Anal.* **3**(2), 103–118 (1999).
6. B. Zheng, Y. H. Chang, and D. Gur, "Computerized detection of masses from digitized mammograms: comparison of single-image segmentation and bilateral-image subtraction," *Acad. Radiol.* **2**(12), 1056–1061 (1995).
7. E. R. Price, B. N. Joe, and E. A. Sickles, "The developing asymmetry: revisiting a perceptual and diagnostic challenge," *Radiology* **274**(3), 642–651 (2015).
8. H. Qi et al., "Detecting breast cancer from infrared images by asymmetry analysis," in *Proc. 22nd Annual Int. Conf. of the IEEE Engineering in Medicine and Biology Society*, Chicago, Illinois, pp. 1227–1228 (2000).
9. G. Schaefer, M. Závisek, and T. Nakashima, "Thermography based breast cancer analysis using statistical features and fuzzy classification," *Pattern Recognit.* **42**(6), 1133–1137 (2009).
10. B. Brooksby et al., "Imaging breast adipose and fibroglandular tissue molecular signatures by using hybrid MRI-guided near-infrared spectral tomography," *Proc. Natl. Acad. Sci. U. S. A.* **103**(23), 8828–8833 (2006).
11. N. Shah et al., "Spatial variations in optical and physiological properties of healthy breast tissue," *J. Biomed. Opt.* **9**(3), 534–540 (2004).
12. A. Cerussi et al., "In vivo absorption, scattering, and physiologic properties of 58 malignant breast tumors determined by broadband diffuse optical spectroscopy," *J. Biomed. Opt.* **11**(4), 044005 (2006).
13. H. Rinneberg et al., "Detection and characterization of breast tumours by time-domain scanning optical mammography," *Optoelectron. Rev.* **16**(2), 147–162 (2008).
14. Q. Fang et al., "Combined optical and x-ray tomosynthesis breast imaging," *Radiology* **258**(1), 89–97 (2011).
15. J. Wang et al., "In vivo quantitative imaging of normal and cancerous breast tissue using broadband diffuse optical tomography," *Med. Phys.* **37**(7), 3715–3724 (2010).
16. X. Intes, "Time-domain optical mammography SoftScan: initial results," *Acad. Radiol.* **12**(8), 934–947 (2005).
17. R. Choe et al., "Differentiation of benign and malignant breast tumors by in-vivo three-dimensional parallel-plate diffuse optical tomography," *J. Biomed. Opt.* **14**(2), 024020 (2009).
18. L. C. Enfield et al., "Three-dimensional time-resolved optical mammography of the uncompressed breast," *Appl. Opt.* **46**(17), 3628–3638 (2007).
19. V. Ntziachristos et al., "MRI-guided diffuse optical spectroscopy of malignant and benign breast lesions," *Neoplasia* **4**(4), 347–354 (2002).
20. B. J. Tromberg et al., "Non-invasive in vivo characterization of breast tumors using photon migration spectroscopy," *Neoplasia* **2**(1–2), 26–40 (2000).
21. S. Srinivasan et al., "Near-infrared characterization of breast tumors in vivo using spectrally-constrained reconstruction," *Technol. Cancer Res. Treat.* **4**(5), 513–526 (2005).
22. Y. Yu et al., "Near-infrared, broad-band spectral imaging of the human breast for quantitative oximetry: applications to healthy and cancerous breasts," *J. Innov. Opt. Health Sci.* **3**(4), 267–277 (2010).
23. L. Spinelli et al., "Characterization of female breast lesions from multi-wavelength time-resolved optical mammography," *Phys. Med. Biol.* **50**(11), 2489–2502 (2005).
24. P. G. Anderson et al., "Broadband optical mammography: chromophore concentration and hemoglobin saturation contrast in breast cancer," *PLoS One* **10**(3), e0117322 (2015).
25. A. Cerussi et al., "Predicting response to breast cancer neoadjuvant chemotherapy using diffuse optical spectroscopy," *Proc. Natl. Acad. Sci. U. S. A.* **104**(10), 4014–4019 (2007).
26. S. Jiang et al., "Evaluation of breast tumor response to neoadjuvant chemotherapy with tomographic diffuse optical spectroscopy: case studies of tumor region-of-interest changes," *Radiology* **252**(2), 551–560 (2009).
27. H. Soliman et al., "Functional imaging using diffuse optical spectroscopy of neoadjuvant chemotherapy response in women with locally advanced breast cancer," *Clin. Cancer Res.* **16**(9), 2605–2614 (2010).
28. D. Roblyer et al., "Optical imaging of breast cancer oxyhemoglobin flare correlates with neoadjuvant chemotherapy response one day after starting treatment," *Proc. Natl. Acad. Sci. U. S. A.* **108**(35), 14626–14631 (2011).

29. A. E. Cerussi et al., "Diffuse optical spectroscopic imaging correlates with final pathological response in breast cancer neoadjuvant chemotherapy," *Philos. Trans. A Math Phys. Eng. Sci.* **369**(1955), 4512–4530 (2011).
30. Q. Zhu et al., "Breast cancer: assessing response to neoadjuvant chemotherapy by using US-guided near-infrared tomography," *Radiology* **266**(2), 433–442 (2013).
31. D. Grosenick et al., "Time-domain scanning optical mammography: II. Optical properties and tissue parameters of 87 carcinomas," *Phys. Med. Biol.* **50**(11), 2451–2468 (2005).
32. D. Contini, F. Martelli, and G. Zaccanti, "Photon migration through a turbid slab described by a model based on diffusion approximation. I. Theory," *Appl. Opt.* **36**(19), 4587–4599 (1997).
33. K. Madsen, H. Nielsen, and O. Tingleff, *Methods for Non-Linear Least Squares Problems*, Technical University of Denmark, Lyngby, Denmark, Lecture Notes (2004).
34. S. R. Arridge and W. R. Lionheart, "Nonuniqueness in diffusion-based optical tomography," *Opt. Lett.* **23**(11), 882–884 (1998).
35. A. Sassaroli et al., "Performance of fitting procedures in curved geometry for retrieval of the optical properties of tissue from time-resolved measurements," *Appl. Opt.* **40**(1), 185–197 (2001).
36. S. Carraresi et al., "Accuracy of a perturbation model to predict the effect of scattering and absorbing inhomogeneities on photon migration," *Appl. Opt.* **40**(25), 4622–4632 (2001).
37. M. Guray and A. A. Sahin, "Benign breast diseases: classification, diagnosis, and management," *Oncologist* **11**(5), 435–449 (2006).
38. W. R. Crum, O. Camara, and D. L. Hill, "Generalized overlap measures for evaluation and validation in medical image analysis," *IEEE Trans. Med. Imaging* **25**(11), 1451–1461 (2006).

Biographies for the authors are not available.